JOURNAL OF MATERIALS PROCESSING TECHNOLOGY 198 (2008) 485–486

available at www.sciencedirect.com

ScienceDirect

journal homepage: www.elsevier.com/locate/jmatprotec

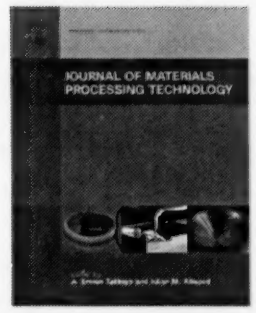

Author Index of Volume 198

Aceves-Hernández, J.M., 162
Ahsan, A.K., 122
Aksoy, T., 183
Al-Hassani, S.T.S., 213
Asgari, H., 54
Azmir, M.A., 122

Bacaksız, E., 202
Balakumar, S., 281
Ballif, C., 105, 114
Barrett, L.M., 213
Barricas, N., 99
Benmaouche, M., 86
Bhaduri, A.K., 73
Bishop, D.P., 31
Bubnovich, V.I., 93
Buchmayr, B., 41
Buchner, B., 41

Çakır, O., 220
Calvet, J.V., 93
Castaño-Meneses, V.M., 162
Cetinel, H., 183
Champliaud, H., 330
Chang, P.-C., 407
Changjun, C., 275
Chen, G., 270
Chen, J.M., 191
Chen, L., 129
Chen, T.-C., 248
Chen, Y.-T., 478
Cheng, X.-n., 270
Chiou, C.-R., 419
Chizari, M., 213
Choi, S., 471
Conceição, M., 99
Correa, E.O., 323
Costa, S.C., 323

Darbandi, P., 381
Darling, R.B., 248
Davim, J.P., 99
Dean, T.A., 48
Debois, D., 226
Dilwith, J.R., 22
Dinc, C., 147
Dongsheng, W., 275
Dunnett, K.S., 31
Durán-Guerrero, S.M., 162
Dutta, B.K., 195

Ebrahimi, R., 48
El-Shall, H., 139
Erdmann, M., 300

Farsani, R.E., 60
Fengying, Z., 454
Francillette, H., 86
Fuchi, W., 207

Gaona, M., 426
Gauquelin, N., 86
Golozar, M.A., 54
González Rojas, H.A., 93
Gracciolli, J.I., 155
Grujicic, M., 300
Gupta, N., 178

Haddad, M.J., 77
Hannon, A., 1
Harp, W.R., 22
Hinojosa-Torres, J., 162
Holzleitner, J., 300
Hsiang, S.M., 313
Hsu, C.Y., 359
Hu, L.T., 191
Hua, T., 454
Huang, B.-W., 350
Huang, K., 129
Huang, M.-S., 436
Hwang, W.-J., 234

Imamura, Y., 234
Islam, M.M., 281

Jansson, M., 14
Jayaraman, K., 168
Jeelani, S., 445
Jin, M., 391
Jing, C., 454
Joo, D.H., 366

Kang, S.-W., 478
Kang, Y., 291
Kannan, S., 399
Karabelchtchikova, O., 313
Kartal, S.N., 234
Katsuhiro, Y., 391
Kilickap, E., 220
Kim, H.-S., 414
Kim, M.H., 366
Kim, Y., 471
Kishawy, H.A., 399
Kumar, A.S., 281
Kurama, S., 68

Labeas, G.N., 260
Lazoglu, I., 147
Le Maoût, N., 226
Lee, B.S., 366
Lee, J.-H., 414
Lee, S.-H., 478
Lee, W.S., 359
Lim, H.S., 281
Lima, R.S., 426
Lin, C.-J., 419
Lin, L.-D., 419
Lin, S.-W., 407
Lin, T.-Y., 436
Lin, Y.Y., 359
Liu, G., 129
Liu, W.M., 191
Liu, Y., 129
Liu, Z., 330
Lo, S.P., 359
Lourençato, L.A., 155
Lu, W., 207
Luccioni, B.M., 372
Luege, M., 372
Lv, C., 463

Maderthoner, G., 41
Mahadevan, K., 241
Maity, K.P., 344
Mallick, P.K., 445
Manach, P.Y., 226
Mandal, D., 195
Maocai, W., 275
Marple, B.R., 426
Mears, L., 300
Michler, J., 105, 114
Miskioğlu, İ, 202
Mohamed, R.M., 139
Moraitis, G.A., 260
Morin, C., 168
Moshksar, M.M., 48
Mu, Z., 463
Mueller, R.M., 31
Murakawa, M., 391

Na, K., 471
Nilsson, L., 14

Elsevier B.V.
doi:10.1016/S0924-0136(07)01394-5

Oliveira, C., 99
Ozben, T., 220
Ozel, E., 68

Pai, B.C., 241
Panigrahi, S.C., 195
Park, J., 471
Park, S.-I., 414
Parsa, M.H., 381
Paydar, M.H., 48
Pecqueux, N., 168
Pervin, F., 445
Pillai, U.T.S., 241
Pouvreau, C., 105, 114
Pürçek, G., 202

Qunbo, F., 207

Raghukandan, K., 241
Rahman, M., 281
Rashad, M.M., 139
Ray, S.K., 73
Reihanian, M., 48
Ren, J., 275
Ricci, W., 178
Rivero, I.V., 313

Santos, J.N., 323
Schulz, D., 105, 114
Sedghi, A., 60
Sellappan, V., 300
Serpenguzel, A., 147
Seyr, N., 300
Shankar, V., 73
Shokuhfar, A., 60
Simonsson, K., 14
Song, J.-H., 414
Song, R., 291
Srinivasan, G., 73
Sun, H.-q., 270
Swain, P.K., 344

Tai, Q., 463
Tehrani, A.F., 77
Thipprakmas, S., 391
Thuillier, S., 226
Tiernan, P., 1
Tomokazu, K., 391
Toroghinejad, M.R., 54
Tsai, C.-H., 350
Tsai, M.-J., 419
Tu, J.F., 22

Wang, M., 134
Wang, Y.-C., 419
Wang, Y.-N., 419
Wasmer, K., 105, 114
Weidong, H., 454
Wu, L.-C., 478

Xin, L., 454
Xu, X., 168
Xu, X.L., 254
Xuan, X., 300

Yiming, L., 275
Yu, Z.W., 254

Zeng, J., 330
Zhang, H., 191
Zhang, L., 463
Zhang, S.-l., 270
Zhang, Y.S., 191
Zhao, A., 291
Zhao, Y., 134
Zhao, Y.-t., 270
Zheng, Q., 463
Zhou, Y., 445
Zoqui, E.J., 155

JOURNAL OF MATERIALS PROCESSING TECHNOLOGY 198 (2008) 487–494

available at www.sciencedirect.com

ScienceDirect

journal homepage: www.elsevier.com/locate/jmatprotec

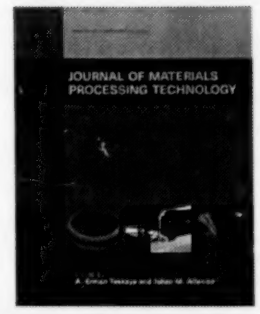

Subject Index of Volume 198

Ablation rate
Laser micromachining of the materials using in microfluidics by high precision pulsed near and mid-ultraviolet Nd:YAG lasers, 248
Adhesion
Structure and nanomechanical properties of CdTe thin films, 202
Aerogel
Processing and compressive properties of aerogel/epoxy composites, 178
AISI 1050
Analysis of thermal fields in orthogonal machining with infrared imaging, 147
AISI D3 tool steel
Investigation of cylindrical wire electrical discharge turning (CWEDT) of AISI D3 tool steel based on statistical analysis, 77
Al7075
Analysis of thermal fields in orthogonal machining with infrared imaging, 147
Al–Cu alloys
Textures and mechanical properties of extruded Al–Cu alloys in the semisolid state, 366
Al–2Mg base composite
Effect of wt% reinforcement on microstructure and mechanical properties of Al–2Mg base short steel fiber composites, 195
Aluminides
Development of Al–Ni–Mg–(Cu) aluminum P/M alloys, 31
Aluminium
Characterisation of different lubricants concerning the friction coefficient in forging of AA2618, 41
Numerical simulation of the roll hemming process, 226
Aluminium alloys
Tube hydroforming of aluminium extrusions using a conical die and extensive feeding, 14
Aluminum alloys
Development of Al–Ni–Mg–(Cu) aluminum P/M alloys, 31
Amorphous
Preparation and electrode behavior of $NdMgNi_{3.6}Co_{0.4}$ hydrogen storage alloy, 270
Anisotropic material
Tube hydroforming of aluminium extrusions using a conical die and extensive feeding, 14
ANOVA
Influence of precipitation hardening parameters on the fatigue strength of AA 6061-SiC_p composite, 241
Austenite
Metallurgical analysis on a bending failed pump-shaft made of 17-7PH precipitation-hardening stainless steel, 254
Auto body parts
Experimental and numerical analyses of sheet hydroforming process for production of an automobile body part, 381
Automotive structural components
Selection of the spraying technologies for over-coating of metal-stampings with thermo-plastics for use in direct-adhesion polymer metal hybrid load-bearing components, 300
AWJM
Investigation on glass/epoxy composite surfaces machined by abrasive water jet machining, 122

Ball milling
Preparation and electrode behavior of $NdMgNi_{3.6}Co_{0.4}$ hydrogen storage alloy, 270
Basal texture component
Relationship between (00.2) and (20.1) texture components and corrosion resistance of hot-dip galvanized zinc coatings, 54
Bending failure
Metallurgical analysis on a bending failed pump-shaft made of 17-7PH precipitation-hardening stainless steel, 254
Biaxial
A review of planar biaxial tensile test systems for sheet metal, 1
Blanking
Prediction of Fineblanked surface characteristics using the finite element method (FEM), 391
Bond strength
Influence of particle temperature and velocity on the microstructure and mechanical behaviour of high velocity oxy-fuel (HVOF)-sprayed nanostructured titania coatings, 426
Boric acid
Combined effect of boron compounds and heat treatments on wood properties: Chemical and strength properties of wood, 234
BUE
Machining characteristics of Inconel 718 using ultrasonic and high temperature-aided cutting, 359
Burr
Some experimental studies on CO_2 laser cutting quality of polymeric materials, 99

Carbon fibers
The effect of commercial polyacrylonitrile fibers characterizations on the produced carbon fibers properties, 60

Elsevier B.V.
doi:10.1016/S0924-0136(07)01395-7

Carbon nanofiber
Improvement in mechanical properties of carbon fabric–epoxy composite using carbon nanofibers, 445
Carbon/epoxy composite
Improvement in mechanical properties of carbon fabric–epoxy composite using carbon nanofibers, 445
Caulking process
Application of FE analysis for optimal design of caulking process, 471
CdTe thin film
Structure and nanomechanical properties of CdTe thin films, 202
Chemical composition
The effect of commercial polyacrylonitrile fibers characterizations on the produced carbon fibers properties, 60
Chemical properties
Combined effect of boron compounds and heat treatments on wood properties: Chemical and strength properties of wood, 234
Citrate precursor method
Magnetic properties of nanocrystalline Sm-substituted $CoFe_2O_4$ synthesized by citrate precursor method, 139
Cladding thickness
Research on molten pool temperature in the process of laser rapid forming, 454
Cleavage
Dicing of gallium–arsenide high performance laser diodes for industrial applications. Part II. Cleavage operation, 105
CMOD
The effect of undermatching on crack tip constraint in a welded structure of nodular irons, 183
CO_2 Laser
Some experimental studies on CO_2 laser cutting quality of polymeric materials, 99
Cobalt ferrite
Magnetic properties of nanocrystalline Sm-substituted $CoFe_2O_4$ synthesized by citrate precursor method, 139
Color difference
Effects of feed speed ratio and laser power on engraved depth and color difference of Moso bamboo lamina, 419
Commercial polyacrylonitrile fibers
The effect of commercial polyacrylonitrile fibers characterizations on the produced carbon fibers properties, 60
Composites
Life cycle assessment of wood-fibre-reinforced polypropylene composites, 168
Tribological aspects of machining aluminium metal matrix composites, 399
Compression
Processing and compressive properties of aerogel/epoxy composites, 178
Computational contact mechanics
Numerical simulation of the lubricant performance in tube hydroforming, 372
Conical rolls
FEM dynamic simulation and analysis of the roll-bending process for forming a conical tube, 330
Conical tabular parts
FEM dynamic simulation and analysis of the roll-bending process for forming a conical tube, 330
Constitutive behaviour
Numerical simulation of the roll hemming process, 226
Controlled fracture
Diamond scribing and laser breaking for LCD glass substrates, 350
Coolant
Tribological aspects of machining aluminium metal matrix composites, 399
Copper-coated steel fiber reinforcement
Effect of wt% reinforcement on microstructure and mechanical properties of Al–2Mg base short steel fiber composites, 195
Cordierite
Production of cordierite ceramic by aqueous tape casting process, 68
Correlation coefficient
Influence of precipitation hardening parameters on the fatigue strength of AA 6061-SiC_p composite, 241
Corrosion resistance
Relationship between (00.2) and (20.1) texture components and corrosion resistance of hot-dip galvanized zinc coatings, 54
Co-sintering
Fabrication characteristics of an anode-supported thin-film electrolyte fabricated by the tape casting method for IT-SOFC, 414
Cracks
Dicing of gallium–arsenide high performance laser diodes for industrial applications. Part I. Scratching operation, 114
Cracks propagation
Dicing of gallium–arsenide high performance laser diodes for industrial applications. Part II. Cleavage operation, 105
Cruciform
A review of planar biaxial tensile test systems for sheet metal, 1
Crystal structure
Microstructural characterization and crystallization of ZrO_2–Y_2O_3–CuO solid solution powders, 191
Crystalline phases
Crystalline phases and granular structure of TIG-welded Zn–22Al–2Cu alloy plates, 162
Cutting variables
An experimental investigation of hot-machining to predict tool life, 344
CWEDT
Investigation of cylindrical wire electrical discharge turning (CWEDT) of AISI D3 tool steel based on statistical analysis, 77

3D rigid-viscoplastic FEM
3D FEM simulation of the multi-stage forging process of a gas turbine compressor blade, 463
Dendritic structure
Crystalline phases and granular structure of TIG-welded Zn–22Al–2Cu alloy plates, 162
Design of experiment
An experimental investigation of hot-machining to predict tool life, 344
Diamond scribing
Diamond scribing and laser breaking for LCD glass substrates, 350
Dicing
Dicing of gallium–arsenide high performance laser diodes for industrial applications. Part II. Cleavage operation, 105

Dicing of gallium–arsenide high performance laser diodes for industrial applications. Part I. Scratching operation, 114
DOE
Investigation of cylindrical wire electrical discharge turning (CWEDT) of AISI D3 tool steel based on statistical analysis, 77
Influence of precipitation hardening parameters on the fatigue strength of AA 6061-SiC_p composite, 241
DOT
Combined effect of boron compounds and heat treatments on wood properties: Chemical and strength properties of wood, 234
Drawing
A new analytical solution for prediction of forward tension in the drawing process, 93

Elastic modulus
Structure and nanomechanical properties of CdTe thin films, 202
Electrode properties
Preparation and electrode behavior of $NdMgNi_{3.6}Co_{0.4}$ hydrogen storage alloy, 270
Elevated temperature tensile testing
Development of Al–Ni–Mg–(Cu) aluminum P/M alloys, 31
ELID grinding
Characterization of ELID grinding process for machining silicon wafers, 281
Engraved depth
Effects of feed speed ratio and laser power on engraved depth and color difference of Moso bamboo lamina, 419
Equal channel angular extrusion
An upper-bound approach for equal channel angular extrusion with circular cross-section, 48
Experimental test
Experimental and numerical study of water jet spot welding, 213
Explicit dynamic FEM
FEM dynamic simulation and analysis of the roll-bending process for forming a conical tube, 330

Fatigue strength
Influence of precipitation hardening parameters on the fatigue strength of AA 6061-SiC_p composite, 241
FE analysis
Application of FE analysis for optimal design of caulking process, 471
FEM
Experimental and numerical analyses of sheet hydroforming process for production of an automobile body part, 381
Fiber laser
Laser ablation using a long-pulsed, high-fluence, CW single-mode fiber laser, 22
Fineblanking
Prediction of Fineblanked surface characteristics using the finite element method (FEM), 391
Finite element method (FEM)
Prediction of Fineblanked surface characteristics using the finite element method (FEM), 391
Finite element simulation
Experimental and numerical study of water jet spot welding, 213
Finite elements
Numerical simulation of the roll hemming process, 226
Flanging
Numerical simulation of the roll hemming process, 226
Fluid pressure
Experimental and numerical analyses of sheet hydroforming process for production of an automobile body part, 381
Forging
Characterisation of different lubricants concerning the friction coefficient in forging of AA2618, 41
Forward tension
A new analytical solution for prediction of forward tension in the drawing process, 93
Friction
Characterisation of different lubricants concerning the friction coefficient in forging of AA2618, 41
Friction law
Numerical simulation of the lubricant performance in tube hydroforming, 372

GaAs
Dicing of gallium–arsenide high performance laser diodes for industrial applications. Part I. Scratching operation, 114
Gallium–arsenide
Dicing of gallium–arsenide high performance laser diodes for industrial applications. Part I. Scratching operation, 114
Gallium–arsenide (GaAs)
Dicing of gallium–arsenide high performance laser diodes for industrial applications. Part II. Cleavage operation, 105
Gas turbine compressor blade
3D FEM simulation of the multi-stage forging process of a gas turbine compressor blade, 463
Glass fibre composite
Investigation on glass/epoxy composite surfaces machined by abrasive water jet machining, 122
Grinding performance
Characterization of ELID grinding process for machining silicon wafers, 281

Heat affected zone (HAZ)
Some experimental studies on CO_2 laser cutting quality of polymeric materials, 99
Heat treatment
Combined effect of boron compounds and heat treatments on wood properties: Chemical and strength properties of wood, 234
Helium leak testing
Vacuum brazing of Inconel 600 sleeve to 316L stainless steel sheath of mineral insulated cable, 73
Hemming
Numerical simulation of the roll hemming process, 226
High pressure and high temperature (HPHT)
Preparation of polycrystalline cBN containing nanodiamond, 134
High velocity oxy-fuel (HVOF)
Influence of particle temperature and velocity on the microstructure and mechanical behaviour of high velocity oxy-fuel (HVOF)-sprayed nanostructured titania coatings, 426
High-energy micro-arc alloying (HEMAA)
Mass transfer trends and the formation of a single deposition spot during high-energy micro-arc alloying of AZ31 Mg alloy, 275
High-temperature vacuum brazing
Vacuum brazing of Inconel 600 sleeve to 316L stainless steel sheath of mineral insulated cable, 73

Hot-dip galvanizing
Relationship between (00.2) and (20.1) texture components and corrosion resistance of hot-dip galvanized zinc coatings, 54
Hot-machining
An experimental investigation of hot-machining to predict tool life, 344
Hydroforming
Tube hydroforming of aluminium extrusions using a conical die and extensive feeding, 14
Hydroforming process
Numerical simulation of the lubricant performance in tube hydroforming, 372
Hydrogen storage
Preparation and electrode behavior of $NdMgNi_{3.6}Co_{0.4}$ hydrogen storage alloy, 270
Hydrothermal synthesis
Synthesis and luminescence properties of YVO_4:Dy^{3+} nanorods, 129

Inconel 718
Machining characteristics of Inconel 718 using ultrasonic and high temperature-aided cutting, 359
Indentation hardness
Structure and nanomechanical properties of CdTe thin films, 202
In-flight particle diagnostics
Influence of particle temperature and velocity on the microstructure and mechanical behaviour of high velocity oxy-fuel (HVOF)-sprayed nanostructured titania coatings, 426
Injection molding
An innovative regression model-based searching method for setting the robust injection molding parameters, 436
Inner tie-rod
Application of FE analysis for optimal design of caulking process, 471
IR
Analysis of thermal fields in orthogonal machining with infrared imaging, 147

J-integral
The effect of undermatching on crack tip constraint in a welded structure of nodular irons, 183

Kaolin
Production of cordierite ceramic by aqueous tape casting process, 68
Keyhole modelling
Residual stress and distortion calculation of laser beam welding for aluminum lap joints, 260

Lap joint
Residual stress and distortion calculation of laser beam welding for aluminum lap joints, 260
Laser ablation
Laser ablation using a long-pulsed, high-fluence, CW single-mode fiber laser, 22
Laser beam welding
Residual stress and distortion calculation of laser beam welding for aluminum lap joints, 260
Laser cladding
Research on molten pool temperature in the process of laser rapid forming, 454
Laser cutting
Diamond scribing and laser breaking for LCD glass substrates, 350
Laser diodes
Dicing of gallium–arsenide high performance laser diodes for industrial applications. Part II. Cleavage operation, 105
Dicing of gallium–arsenide high performance laser diodes for industrial applications. Part I. Scratching operation, 114
Laser engraving
Effects of feed speed ratio and laser power on engraved depth and color difference of Moso bamboo lamina, 419
Laser micromachining
Laser micromachining of the materials using in microfluidics by high precision pulsed near and mid-ultraviolet Nd:YAG lasers, 248
Laser rapid forming
Research on molten pool temperature in the process of laser rapid forming, 454
LCD glass
Diamond scribing and laser breaking for LCD glass substrates, 350
Lead content
Relationship between (00.2) and (20.1) texture components and corrosion resistance of hot-dip galvanized zinc coatings, 54
Life cycle assessment
Life cycle assessment of wood-fibre-reinforced polypropylene composites, 168
Light-guided plates
An innovative regression model-based searching method for setting the robust injection molding parameters, 436
Linear regression
Investigation on glass/epoxy composite surfaces machined by abrasive water jet machining, 122
Liquid phase sintering
Development of Al–Ni–Mg–(Cu) aluminum P/M alloys, 31
Low-temperature bonding technique
Fabrication and investigation of PDMS micro-diffuser/nozzle, 478
Lubrication
Numerical simulation of the lubricant performance in tube hydroforming, 372

Machining
Investigation of mechanical and machinability properties of SiC particle reinforced Al-MMC, 220
Machining silicon wafers
Characterization of ELID grinding process for machining silicon wafers, 281
Magnesium alloys
Mass transfer trends and the formation of a single deposition spot during high-energy micro-arc alloying of AZ31 Mg alloy, 275
Magnetic properties
Magnetic properties of nanocrystalline Sm-substituted $CoFe_2O_4$ synthesized by citrate precursor method, 139
Mathematical model
Evaluation of the profile of the taper ball-end milling cutter with a cylindrical shank, 407
Mechanical properties
The effect of commercial polyacrylonitrile fibers characterizations on the produced carbon fibers properties, 60
Investigation of mechanical and machinability properties of SiC particle reinforced Al-MMC, 220

Improvement in mechanical properties of carbon fabric–epoxy composite using carbon nanofibers, 445
Melt extrusion
Textures and mechanical properties of extruded Al–Cu alloys in the semisolid state, 366
Melt-in-welded joints
Crystalline phases and granular structure of TIG-welded Zn–22Al–2Cu alloy plates, 162
Metal matrix composite
Influence of precipitation hardening parameters on the fatigue strength of AA 6061-SiC_p composite, 241
Metals and alloys
Thixo-formability of the AA6063 alloy: Conventional production processes versus electromagnetic stirring, 155
Micro-drilling
Laser ablation using a long-pulsed, high-fluence, CW single-mode fiber laser, 22
Microfluidic
Laser micromachining of the materials using in microfluidics by high precision pulsed near and mid-ultraviolet Nd:YAG lasers, 248
Microstructure
Thixo-formability of the AA6063 alloy: Conventional production processes versus electromagnetic stirring, 155
Influence of particle temperature and velocity on the microstructure and mechanical behaviour of high velocity oxy-fuel (HVOF)-sprayed nanostructured titania coatings, 426
Microstructure and mechanical properties
Effect of wt% reinforcement on microstructure and mechanical properties of Al–2Mg base short steel fiber composites, 195
Minimum circumscribed cylindrical surface (MCCS)
Evaluation of the profile of the taper ball-end milling cutter with a cylindrical shank, 407
Minimum circumscribed sphere (MCS)
Evaluation of the profile of the taper ball-end milling cutter with a cylindrical shank, 407
Minimum circumscribed taper surface (MCTS)
Evaluation of the profile of the taper ball-end milling cutter with a cylindrical shank, 407
MMC
Investigation of mechanical and machinability properties of SiC particle reinforced Al-MMC, 220
Modeling
Modeling of residual stress distribution in D2 steel via grinding dynamics using a second-order damping system, 313
MOE
Combined effect of boron compounds and heat treatments on wood properties: Chemical and strength properties of wood, 234
Molding structure
Fabrication and investigation of PDMS micro-diffuser/nozzle, 478
Molten pool temperature
Research on molten pool temperature in the process of laser rapid forming, 454
MOR
Combined effect of boron compounds and heat treatments on wood properties: Chemical and strength properties of wood, 234
Moso bamboo
Effects of feed speed ratio and laser power on engraved depth and color difference of Moso bamboo lamina, 419
MRR
Investigation of cylindrical wire electrical discharge turning (CWEDT) of AISI D3 tool steel based on statistical analysis, 77
Multipass grinding
Modeling of residual stress distribution in D2 steel via grinding dynamics using a second-order damping system, 313
Multi-stage forging
3D FEM simulation of the multi-stage forging process of a gas turbine compressor blade, 463

Nanocomposites
Microstructural characterization and crystallization of ZrO_2–Y_2O_3–CuO solid solution powders, 191
Nanodiamond
Preparation of polycrystalline cBN containing nanodiamond, 134
Nanopowders
Magnetic properties of nanocrystalline Sm-substituted $CoFe_2O_4$ synthesized by citrate precursor method, 139
Nanostructured titania (TiO_2)
Influence of particle temperature and velocity on the microstructure and mechanical behaviour of high velocity oxy-fuel (HVOF)-sprayed nanostructured titania coatings, 426
Natural fibre composite
Life cycle assessment of wood-fibre-reinforced polypropylene composites, 168
$NdMgNi_{3.6}Co_{0.4}$ alloy
Preparation and electrode behavior of $NdMgNi_{3.6}Co_{0.4}$ hydrogen storage alloy, 270
Nodular iron
The effect of undermatching on crack tip constraint in a welded structure of nodular irons, 183
Non-dendritic
Semi-solid rolling process of steel strips, 291

Operation parameters
Modeling influence of basic operation parameters on plasma jet, 207
Optimal design
Application of FE analysis for optimal design of caulking process, 471

PDMS
Fabrication and investigation of PDMS micro-diffuser/nozzle, 478
17-7PH stainless steel
Metallurgical analysis on a bending failed pump-shaft made of 17-7PH precipitation-hardening stainless steel, 254
Photoluminescence
Synthesis and luminescence properties of YVO_4:Dy^{3+} nanorods, 129
Plasma arc welding
Weldability of iron-based powder metal materials using pulsed plasma arc welding process, 323
Plasma spray
Modeling influence of basic operation parameters on plasma jet, 207
Plastic deformation
Anisotropic behavior of a Ti–6Al–4V sheet during cold rolling: Evidence of macroscopic shearing, 86
Polycrystalline cubic boron nitride (PcBN)
Preparation of polycrystalline cBN containing nanodiamond, 134

Polymer coating processes
Selection of the spraying technologies for over-coating of metal-stampings with thermo-plastics for use in direct-adhesion polymer metal hybrid load-bearing components, 300
Polymer matrix composite
Processing and compressive properties of aerogel/epoxy composites, 178
Polymer metal adhesion
Selection of the spraying technologies for over-coating of metal-stampings with thermo-plastics for use in direct-adhesion polymer metal hybrid load-bearing components, 300
Polymer metal hybrids
Selection of the spraying technologies for over-coating of metal-stampings with thermo-plastics for use in direct-adhesion polymer metal hybrid load-bearing components, 300
Polymeric materials
Some experimental studies on CO_2 laser cutting quality of polymeric materials, 99
Polypropylene
Life cycle assessment of wood-fibre-reinforced polypropylene composites, 168
Powder metal alloys
Weldability of iron-based powder metal materials using pulsed plasma arc welding process, 323
Powder metallurgy
Development of Al–Ni–Mg–(Cu) aluminum P/M alloys, 31
Pressure loss coefficient
Fabrication and investigation of PDMS micro-diffuser/nozzle, 478
Processing
Dicing of gallium–arsenide high performance laser diodes for industrial applications. Part II. Cleavage operation, 105
Dicing of gallium–arsenide high performance laser diodes for industrial applications. Part I. Scratching operation, 114
Processing parameters
Some experimental studies on CO_2 laser cutting quality of polymeric materials, 99
Pump-shaft
Metallurgical analysis on a bending failed pump-shaft made of 17-7PH precipitation-hardening stainless steel, 254

Ra
Investigation of cylindrical wire electrical discharge turning (CWEDT) of AISI D3 tool steel based on statistical analysis, 77
Rake angle
Analysis of thermal fields in orthogonal machining with infrared imaging, 147
Rare earth elements
Magnetic properties of nanocrystalline Sm-substituted $CoFe_2O_4$ synthesized by citrate precursor method, 139
Regression model
An innovative regression model-based searching method for setting the robust injection molding parameters, 436
Residual stress
Modeling of residual stress distribution in D2 steel via grinding dynamics using a second-order damping system, 313
Robustness
An innovative regression model-based searching method for setting the robust injection molding parameters, 436
Roll-bending
FEM dynamic simulation and analysis of the roll-bending process for forming a conical tube, 330
Rolling
Anisotropic behavior of a Ti–6Al–4V sheet during cold rolling: Evidence of macroscopic shearing, 86
Semi-solid rolling process of steel strips, 291
Roundness
Investigation of cylindrical wire electrical discharge turning (CWEDT) of AISI D3 tool steel based on statistical analysis, 77
RSM
Investigation of cylindrical wire electrical discharge turning (CWEDT) of AISI D3 tool steel based on statistical analysis, 77

Scratching
Dicing of gallium–arsenide high performance laser diodes for industrial applications. Part I. Scratching operation, 114
Secondary shear surface
Prediction of Fineblanked surface characteristics using the finite element method (FEM), 391
Self-sharpening ability
Characterization of ELID grinding process for machining silicon wafers, 281
Semiconductors III–V
Dicing of gallium–arsenide high performance laser diodes for industrial applications. Part II. Cleavage operation, 105
Dicing of gallium–arsenide high performance laser diodes for industrial applications. Part I. Scratching operation, 114
Semisolid
Semi-solid rolling process of steel strips, 291
Textures and mechanical properties of extruded Al–Cu alloys in the semisolid state, 366
Semi-solid state processing
Thixo-formability of the AA6063 alloy: Conventional production processes versus electromagnetic stirring, 155
Severe plastic deformation
An upper-bound approach for equal channel angular extrusion with circular cross-section, 48
Shear surface
Prediction of Fineblanked surface characteristics using the finite element method (FEM), 391
Shearing
Anisotropic behavior of a Ti–6Al–4V sheet during cold rolling: Evidence of macroscopic shearing, 86
Sheet hydroforming
Experimental and numerical analyses of sheet hydroforming process for production of an automobile body part, 381
Sheet metal
A review of planar biaxial tensile test systems for sheet metal, 1
Simulation
FEM dynamic simulation and analysis of the roll-bending process for forming a conical tube, 330
Single deposition spot
Mass transfer trends and the formation of a single deposition spot during high-energy micro-arc alloying of AZ31 Mg alloy, 275
Sintering
Preparation of polycrystalline cBN containing nanodiamond, 134

Slab method
A new analytical solution for prediction of forward tension in the drawing process, 93
Solid content
Production of cordierite ceramic by aqueous tape casting process, 68
Solid oxide fuel cell (SOFC)
Fabrication characteristics of an anode-supported thin-film electrolyte fabricated by the tape casting method for IT-SOFC, 414
Spangle size
Relationship between (00.2) and (20.1) texture components and corrosion resistance of hot-dip galvanized zinc coatings, 54
Species distribution
Modeling influence of basic operation parameters on plasma jet, 207
Specimens
A review of planar biaxial tensile test systems for sheet metal, 1
Splash and gasification
Mass transfer trends and the formation of a single deposition spot during high-energy micro-arc alloying of AZ31 Mg alloy, 275
Spot welding
Experimental and numerical study of water jet spot welding, 213
Stabilization
The effect of commercial polyacrylonitrile fibers characterizations on the produced carbon fibers properties, 60
Stamping
Experimental and numerical analyses of sheet hydroforming process for production of an automobile body part, 381
Steel
Semi-solid rolling process of steel strips, 291
Steepest ascent method
An innovative regression model-based searching method for setting the robust injection molding parameters, 436
Stress triaxiality
The effect of undermatching on crack tip constraint in a welded structure of nodular irons, 183
Strip
Semi-solid rolling process of steel strips, 291
SU-8
Fabrication and investigation of PDMS micro-diffuser/nozzle, 478
Superposition
Modeling of residual stress distribution in D2 steel via grinding dynamics using a second-order damping system, 313
Surface roughness
Investigation of mechanical and machinability properties of SiC particle reinforced Al-MMC, 220

Taguchi's method
Investigation on glass/epoxy composite surfaces machined by abrasive water jet machining, 122
Machining characteristics of Inconel 718 using ultrasonic and high temperature-aided cutting, 359
Tape-casting
Production of cordierite ceramic by aqueous tape casting process, 68
Fabrication characteristics of an anode-supported thin-film electrolyte fabricated by the tape casting method for IT-SOFC, 414
Taper ball-end milling cutter
Evaluation of the profile of the taper ball-end milling cutter with a cylindrical shank, 407
Tearing
Prediction of Fineblanked surface characteristics using the finite element method (FEM), 391
Temperature
Analysis of thermal fields in orthogonal machining with infrared imaging, 147
Temperature field
Modeling influence of basic operation parameters on plasma jet, 207
Temperature measure
Research on molten pool temperature in the process of laser rapid forming, 454
Testing
A review of planar biaxial tensile test systems for sheet metal, 1
Texture
Anisotropic behavior of a Ti–6Al–4V sheet during cold rolling: Evidence of macroscopic shearing, 86
Textures and mechanical properties of extruded Al–Cu alloys in the semisolid state, 366
Thermal ablation
Laser ablation using a long-pulsed, high-fluence, CW single-mode fiber laser, 22
Thermal cycle
Vacuum brazing of Inconel 600 sleeve to 316L stainless steel sheath of mineral insulated cable, 73
Thermal degradation
Combined effect of boron compounds and heat treatments on wood properties: Chemical and strength properties of wood, 234
Thermal dilatometry
Development of Al–Ni–Mg–(Cu) aluminum P/M alloys, 31
Thermal spray
Influence of particle temperature and velocity on the microstructure and mechanical behaviour of high velocity oxy-fuel (HVOF)-sprayed nanostructured titania coatings, 426
Thermo-mechanical analysis
Residual stress and distortion calculation of laser beam welding for aluminum lap joints, 260
Thin-film electrolyte
Fabrication characteristics of an anode-supported thin-film electrolyte fabricated by the tape casting method for IT-SOFC, 414
TIG welding
Crystalline phases and granular structure of TIG-welded Zn–22Al–2Cu alloy plates, 162
Tool life
An experimental investigation of hot-machining to predict tool life, 344
Tool wear
Investigation of mechanical and machinability properties of SiC particle reinforced Al-MMC, 220
Triaxial mineral insulated cable
Vacuum brazing of Inconel 600 sleeve to 316L stainless steel sheath of mineral insulated cable, 73
Turning
Tribological aspects of machining aluminium metal matrix composites, 399

Ultrasonic vibration
Machining characteristics of Inconel 718 using ultrasonic and high temperature-aided cutting, 359

Ultraviolet laser
Laser micromachining of the materials using in microfluidics by high precision pulsed near and mid-ultraviolet Nd:YAG lasers, 248
Undermatching
The effect of undermatching on crack tip constraint in a welded structure of nodular irons, 183
Upper-bound theory
An upper-bound approach for equal channel angular extrusion with circular cross-section, 48

Velocity
Analysis of thermal fields in orthogonal machining with infrared imaging, 147
Velocity field
Modeling influence of basic operation parameters on plasma jet, 207

Water jet
Experimental and numerical study of water jet spot welding, 213
Weldability
Weldability of iron-based powder metal materials using pulsed plasma arc welding process, 323
Welding simulation
Residual stress and distortion calculation of laser beam welding for aluminum lap joints, 260
Wire EDM
Investigation of cylindrical wire electrical discharge turning (CWEDT) of AISI D3 tool steel based on statistical analysis, 77
Wood-fibre
Life cycle assessment of wood-fibre-reinforced polypropylene composites, 168

YVO_4
Synthesis and luminescence properties of YVO_4:Dy^{3+} nanorods, 129

Zn–22Al–2Cu (weight %) alloy
Crystalline phases and granular structure of TIG-welded Zn–22Al–2Cu alloy plates, 162
ZrO_2–Y_2O_3–CuO
Microstructural characterization and crystallization of ZrO_2–Y_2O_3–CuO solid solution powders, 191

ELSEVIER

Volume 198, Issues 1–3, 3 March 2008

Journal of
Materials
Processing
Technology

www.elsevier.com/locate/jmatprotec

Contents

A review of planar biaxial tensile test systems for sheet metal 1
A. Hannon, P. Tiernan

Tube hydroforming of aluminium extrusions using a conical die and extensive feeding..... 14
M. Jansson, L. Nilsson, K. Simonsson

Laser ablation using a long-pulsed, high-fluence, CW single-mode fiber laser 22
W.R. Harp, J.R. Dilwith, J.F. Tu

Development of Al–Ni–Mg–(Cu) aluminum P/M alloys 31
K.S. Dunnett, R.M. Mueller, D.P. Bishop

Characterisation of different lubricants concerning the friction coefficient in forging of AA2618 41
B. Buchner, G. Maderthoner, B. Buchmayr

An upper-bound approach for equal channel angular extrusion with circular cross-section 48
M.H. Paydar, M. Reihanian, R. Ebrahimi, T.A. Dean, M.M. Moshksar

Relationship between (00.2) and (20.1) texture components and corrosion resistance of hot-dip galvanized zinc coatings..... 54
H. Asgari, M.R. Toroghinejad, M.A. Golozar

The effect of commercial polyacrylonitrile fibers characterizations on the produced carbon fibers properties..... 60
A. Sedghi, R.E. Farsani, A. Shokuhfar

Production of cordierite ceramic by aqueous tape casting process..... 68
E. Ozel, S. Kurama

Vacuum brazing of Inconel 600 sleeve to 316L stainless steel sheath of mineral insulated cable..... 73
G. Srinivasan, A.K. Bhaduri, S.K. Ray, V. Shankar

Investigation of cylindrical wire electrical discharge turning (CWEDT) of AISI D3 tool steel based on statistical analysis 77
M.J. Haddad, A.F. Tehrani

Anisotropic behavior of a Ti–6Al–4V sheet during cold rolling: Evidence of macroscopic shearing..... 86
H. Francillette, M. Benmaouche, N. Gauquelin

A new analytical solution for prediction of forward tension in the drawing process..... 93
H.A. González Rojas, J.V. Calvet, V.I. Bubnovich

Some experimental studies on CO_2 laser cutting quality of polymeric materials..... 99
J.P. Davim, N. Barricas, M. Conceição, C. Oliveira

Dicing of gallium–arsenide high performance laser diodes for industrial applications. Part II. Cleavage operation..... 105
K. Wasmer, C. Ballif, C. Pouvreau, D. Schulz, J. Michler

Dicing of gallium–arsenide high performance laser diodes for industrial applications. Part I. Scratching operation 114
K. Wasmer, C. Ballif, C. Pouvreau, D. Schulz, J. Michler

Investigation on glass/epoxy composite surfaces machined by abrasive water jet machining..... 122
M.A. Azmir, A.K. Ahsan

Synthesis and luminescence properties of $YVO_4:Dy^{3+}$ nanorods..... 129
L. Chen, G. Liu, Y. Liu, K. Huang

Preparation of polycrystalline cBN containing nanodiamond 134
Y. Zhao, M. Wang

(Contents continued on page I)

0924-0136(20080303)198:1/3;1-Q

6017

(Contents continued from OBC)

Magnetic properties of nanocrystalline Sm-substituted $CoFe_2O_4$ synthesized by citrate precursor method ... 139
M.M. Rashad, R.M. Mohamed, H. El-Shall

Analysis of thermal fields in orthogonal machining with infrared imaging ... 147
C. Dinc, I. Lazoglu, A. Serpenguzel

Thixo-formability of the AA6063 alloy: Conventional production processes versus electromagnetic stirring ... 155
E.J. Zoqui, J.I. Gracciolli, L.A. Lourençato

Crystalline phases and granular structure of TIG-welded Zn–22Al–2Cu alloy plates ... 162
J. Hinojosa-Torres, S.M. Durán-Guerrero, J.M. Aceves-Hernández, V.M. Castaño-Meneses

Life cycle assessment of wood-fibre-reinforced polypropylene composites ... 168
X. Xu, K. Jayaraman, C. Morin, N. Pecqueux

Processing and compressive properties of aerogel/epoxy composites ... 178
N. Gupta, W. Ricci

The effect of undermatching on crack tip constraint in a welded structure of nodular irons ... 183
H. Cetinel, T. Aksoy

Microstructural characterization and crystallization of ZrO_2–Y_2O_3–CuO solid solution powders ... 191
Y.S. Zhang, L.T. Hu, H. Zhang, J.M. Chen, W.M. Liu

Effect of wt% reinforcement on microstructure and mechanical properties of Al–2Mg base short steel fiber composites ... 195
D. Mandal, B.K. Dutta, S.C. Panigrahi

Structure and nanomechanical properties of CdTe thin films ... 202
G. Pürçek, E. Bacaksız, İ. Miskioğlu

Modeling influence of basic operation parameters on plasma jet ... 207
F. Qunbo, W. Lu, W. Fuchi

Experimental and numerical study of water jet spot welding ... 213
M. Chizari, S.T.S. Al-Hassani, L.M. Barrett

Investigation of mechanical and machinability properties of SiC particle reinforced Al-MMC ... 220
T. Ozben, E. Kilickap, O. Çakır

Numerical simulation of the roll hemming process ... 226
S. Thuillier, N. Le Maoût, P.Y. Manach, D. Debois

Combined effect of boron compounds and heat treatments on wood properties: Chemical and strength properties of wood ... 234
S.N. Kartal, W.-J. Hwang, Y. Imamura

Influence of precipitation hardening parameters on the fatigue strength of AA 6061-SiC_p composite ... 241
K. Mahadevan, K. Raghukandan, B.C. Pai, U.T.S. Pillai

Laser micromachining of the materials using in microfluidics by high precision pulsed near and mid-ultraviolet Nd:YAG lasers ... 248
T.-C. Chen, R.B. Darling

Metallurgical analysis on a bending failed pump-shaft made of 17-7PH precipitation-hardening stainless steel ... 254
X.L. Xu, Z.W. Yu

Residual stress and distortion calculation of laser beam welding for aluminum lap joints ... 260
G.A. Moraitis, G.N. Labeas

Preparation and electrode behavior of $NdMgNi_{3.6}Co_{0.4}$ hydrogen storage alloy ... 270
S.-l. Zhang, Y.-t. Zhao, G. Chen, X.-n. Cheng, H.-q. Sun

Mass transfer trends and the formation of a single deposition spot during high-energy micro-arc alloying of AZ31 Mg alloy ... 275
C. Changjun, W. Maocai, L. Yiming, W. Dongsheng, J. Ren

Characterization of ELID grinding process for machining silicon wafers ... 281
M.M. Islam, A.S. Kumar, S. Balakumar, H.S. Lim, M. Rahman

Semi-solid rolling process of steel strips ... 291
R. Song, Y. Kang, A. Zhao

Selection of the spraying technologies for over-coating of metal-stampings with thermo-plastics for use in direct-adhesion polymer metal hybrid load-bearing components 300
M. Grujicic, V. Sellappan, L. Mears, X. Xuan, N. Seyr, M. Erdmann, J. Holzleitner

Modeling of residual stress distribution in D2 steel via grinding dynamics using a second-order damping system 313
O. Karabelchtchikova, I.V. Rivero, S.M. Hsiang

Weldability of iron-based powder metal materials using pulsed plasma arc welding process..... 323
E.O. Correa, S.C. Costa, J.N. Santos

FEM dynamic simulation and analysis of the roll-bending process for forming a conical tube..... 330
J. Zeng, Z. Liu, H. Champliaud

An experimental investigation of hot-machining to predict tool life 344
K.P. Maity, P.K. Swain

Diamond scribing and laser breaking for LCD glass substrates 350
C.-H. Tsai, B.-W. Huang

Machining characteristics of Inconel 718 using ultrasonic and high temperature-aided cutting..... 359
C.Y. Hsu, Y.Y. Lin, W.S. Lee, S.P. Lo

Textures and mechanical properties of extruded Al–Cu alloys in the semisolid state..... 366
B.S. Lee, D.H. Joo, M.H. Kim

Numerical simulation of the lubricant performance in tube hydroforming 372
M. Luege, B.M. Luccioni

Experimental and numerical analyses of sheet hydroforming process for production of an automobile body part..... 381
M.H. Parsa, P. Darbandi

Prediction of Fineblanked surface characteristics using the finite element method (FEM)..... 391
S. Thipprakmas, M. Jin, K. Tomokazu, Y. Katsuhiro, M. Murakawa

Tribological aspects of machining aluminium metal matrix composites..... 399
S. Kannan, H.A. Kishawy

Evaluation of the profile of the taper ball-end milling cutter with a cylindrical shank..... 407
P.-C. Chang, S.-W. Lin

Fabrication characteristics of an anode-supported thin-film electrolyte fabricated by the tape casting method for IT-SOFC 414
J.-H. Song, S.-I. Park, J.-H. Lee, H.-S. Kim

Effects of feed speed ratio and laser power on engraved depth and color difference of Moso bamboo lamina... 419
C.-J. Lin, Y.-C. Wang, L.-D. Lin, C.-R. Chiou, Y.-N. Wang, M.-J. Tsai

Influence of particle temperature and velocity on the microstructure and mechanical behaviour of high velocity oxy-fuel (HVOF)-sprayed nanostructured titania coatings..... 426
M. Gaona, R.S. Lima, B.R. Marple

An innovative regression model-based searching method for setting the robust injection molding parameters 436
M.-S. Huang, T.-Y. Lin

Improvement in mechanical properties of carbon fabric–epoxy composite using carbon nanofibers 445
Y. Zhou, F. Pervin, S. Jeelani, P.K. Mallick

Research on molten pool temperature in the process of laser rapid forming..... 454
T. Hua, C. Jing, L. Xin, Z. Fengying, H. Weidong

3D FEM simulation of the multi-stage forging process of a gas turbine compressor blade..... 463
C. Lv, L. Zhang, Z. Mu, Q. Tai, Q. Zheng

Application of FE analysis for optimal design of caulking process 471
J. Park, J. Park, S. Choi, K. Na, Y. Kim

Fabrication and investigation of PDMS micro-diffuser/nozzle 478
Y.-T. Chen, S.-W. Kang, L.-C. Wu, S.-H. Lee

Author index..... 485

Subject index 487